Hindawi
Advances in Civil Engineering
Volume 2022, Article ID 2840318, 9 pages
https://doi.org/10.1155/2022/2840318

Research Article

Evaluating the Properties of Railway Ballast Using Spectral Analysis of Ground Penetrating Radar Signal Based on Optimized Variational Mode Decomposition

Wael Zatar,[1] Xia Hua ,[2] Gang Chen,[1] Hai Nguyen,[1] and Hien Nghiem[1]

[1]*College of Engineering and Computer Sciences, Marshall University, Huntington, WV 25755, USA*
[2]*College of Mechanical Engineering, Zhejiang University of Technology, Hangzhou, Zhejiang 310023, China*

Correspondence should be addressed to Xia Hua; huaxia@zjut.edu.cn

Received 16 May 2022; Revised 19 August 2022; Accepted 29 August 2022; Published 10 October 2022

Academic Editor: Jose Matos

Ground penetrating radar (GPR) has been widely applied in the assessment of railway ballast conditions (fouling, moisture) by using the spectrum of the tested GPR signal. However, the drawbacks of the low time-frequency resolution and mode mixing prevent the traditional spectrum methods from a wide application. This paper uses the advanced time-frequency analysis of GPR signal based on optimized variational mode decomposition to extract the features of ballast. The new approach overperforms the conventional frequency spectrum methods of GPR signal processing by giving a clear and quantitative assessment of ballast signals. Experimental results of GPR with dry and wet fouled ballasts demonstrate that, by comparison with the feature extraction method of conventional spectrum methods such as spectrogram and wavelet, the feature extraction method based on the optimized VMD has much better separability and quantitative identification capability.

1. Introduction

The structure of a railway track typically consists of a superstructure and a substructure. The load of the track needs support. Ballast, which is part from the substructure, is the key element to support and transfer the load. Ballast typically consists of angular aggregate that is uniformly graded to provide enough structural capacity and air voids. In practice, rails and sleepers need a relatively dry environment to maintain its maximum performance, and air voids can reduce water drainage and keep the rails and sleepers away from moisture. Over time, general steps to produce ballast were gradually fouling fine materials when filling the air voids; however, the strength and drainage capabilities were compromised. The moisture in the fouling material tends to exacerbate the decrease in strength [1–4]. Ground-penetrating radar (GPR) has been used as a viable technique for quick and nondestructive inspection of the actual condition of railway ballasts [4, 5]. GPR has the ability to produce geophysical images in the following ways. Firstly, GPR measures reflected electromagnetic (EM) waves transmitted in the form of radar pulses in the microwave band of the radio spectrum. Then, a transmitting di-pole antenna radiates EM pulses into the ground, and a receiving dipole antenna measures variations in the reflected signal in a time-domain profile. Finally, the structural properties of the ballast can be inferred from the responses given by those interface reflections. Particularly, using GPR can estimate and monitor the track stiffness indirectly by detecting the ballast layer which is the most important and dominant component in track stiffness. The research has demonstrated the relationship between the parameter of track stiffness with ballast layer and subgrade condition, which shows the promising future use of GPR to estimate the track load carrying capability [1–5]. GPR has been used to quantify the ballast fouling. If the fouling procedure is contaminated by other fines, the mechanical properties of the ballast will be degraded, which will finally lead the railway track into an unstable condition. The research presents the results of experimental studies on the strong relationship between

ballast stiffness and clay fouling. The ballast stiffness is decreased with the increased severity of fouling. GPR time-domain signal of ballast has been used to generate an assessment index for fouling evaluation. Time-domain analysis does not consider the frequency-dispersive properties of ballast media and the signal phase; however, it is easy to filter out electromagnetic interference in the frequency domain. Many attempts used the frequency spectrum analysis to detect the fouling level of ballast, thanks to the Fourier transform, and time-domain GPR data can be successfully converted to the frequency domain. Silvast et al. [6] showed that in a clean ballast, the area of a signal spectrum in the frequency domain is bigger than that of fouled ballast. Leng and Al-Qadi [7] used the short-time Fourier transform (STSF) to investigate the time variation of the frequency spectrum of the GPR signal. They graphically demonstrated the variation of the frequency energy with the ballast depth under different fouling conditions and used the STFT approach on GPR data to quantify railroad ballast fouling, and the result showed that the time-frequency technique was able to reveal changes in ballast fouling over depth. Shao et al. [8] used GPR to evaluate the track ballast conditions at the network level [8]. They proposed a method that used the maximum peak of the spectrum of the frequency domain to automatically assess the condition of ballast and developed an algorithm that can extract magnitude spectra at salient frequencies and classify ballast conditions by support vector machines. Al-Qadi et al. [9] interpreted GPR data and evaluated the fouling of the ballast by a wavelet transform (WT) technique invented by themselves. Then, they summarized and compared processing techniques for time-frequency GPR signal that can be used to evaluate the level of railway ballast fouling. Bianchini Ciampoli et al. [10] analyzed the spectral data of GPR and assessed the geometric properties of the ballast. Fontul et al. [11] investigated and assessed the railway track condition at the network level in the frequency domain using GPR data. They quantified the shift and deformation of the frequency spectrum with changing ballast parameters such as aggregate size and then illustrated the maximum shift of frequency spectrum, regarding them as a function of the dimension of the aggregate particles. The above methodologies revealed a good reliability and effectiveness in monitoring the ballast health. The possibility of characterizing the ballast stiffness can also be proved. Recent related work can be found in [12].

For classifying the ballast, results from existing experiments showed that many approaches are efficient enough to represent and analyze GPR signals. Furthermore, when it comes to the classification of patterns, typical and important features can be extracted from those approaches. Therefore, it can be concluded that GPR is an effective and efficient tool to evaluate the thickness and fouling levels of ballast.

Correlations between GPR parameters, such as the dielectric permittivity and the area of the frequency spectrum as well as the fouling level, have been concluded and assured by previous studies and experiments. However, it is difficult to find efficient methods or specifications to quantify the level of fouling of the ballast. In one word, it is still challenging to determine the level and type of the fouling of the ballast layer from GPR analysis.

With the help of joint time-frequency analysis (JTFA), interpretation of GPR data was no longer a heavy task. However, a lot of traditional JTFA methods, including STFT and WT, were limited in application because low time-frequency (TF) resolution and mode mixing cannot be solved perfectly. Although the most popular tools for JTFA are based on the Fourier transform method, under the limitation of the uncertainty principle, however, these methods cannot be used to analyze the GPR signal because they failed to show the information about the local frequency variations.

Recently, the variational mode decomposition (VMD), which encompasses multiple adaptive Wiener filter groups, has been widely used to process GPR signal, because it showed a good robustness in overcoming the disadvantages of mode aliasing, small end effects, and pseudocomponents when compared to other traditional TF analysis algorithms for GPR [13, 14]. This innovative VMD method also has a solid theoretical foundation in decomposing the adaptive and quasiorthogonal signals [15]. In solving problems, such as mode-mixing, noises, and samplings, VMD successfully shows its advantages in effectiveness and robustness compared to the conventional time-frequency methods. For time-frequency resolution, the VMD-based spectrum can provide a higher resolution, which also performs better than conventional JTFA methods. Sensitivity to data is another feature of the VMD method. In other words, the decomposition parameters, which include the number of extracted modes and are a critical factor for the performance of the method, were determined mainly through the engineering experience. Those inaccurate operations will cause a low method performance, and thus, the accuracy of the outcome will be compromised. Therefore, it is crucial to find an effective and accurate way to determine the parameter. Liu et al. [16] proposed a new approach to choose the parameter and analyze the signals. In his research, he firstly found out the eddy current signal and the frequency spectrum of it, and then, he chooses the number of extracted modes based on the peak point of the spectrum. Next, he analyzed the correlation coefficient between the original and rebuilt signal in mechanical rotor system diagnosis. Shi and Yang [17] developed a revised VMD method for the vibration signals of a wind turbine, and they optimized the number of extracted modes [17]. Isham et al. reviewed a variety of improved VMD and wide applications in rotating machinery diagnosis [18]. Particularly, Li et al. [19] developed a genetic algorithm-based VMD and applied it in fault diagnosis recently [19], and they developed an advanced optimization method for system diagnosis and recognition [20]. Ni et al. [21] developed a fault information-guided VMD (FIVMD) method for extracting weak signals to minimize the effects of background noise and/or interferences [21].

In this research, we choose the optimized VMD-based TF analysis method for ballast GPR signal processing, because it performs better than the conventional JTFA and WT

methods. In other words, the method we choose can accurately capture the spectral features; thus, the TF resolution can be higher, and the TF spectrogram of the GPR signal based on optimized VMD can be much smoother and sparser. The implemented optimized VMD algorithm was chosen to calculate the modes of the original nonlinear GPR signal of railway ballast collected in Huntington, WV in Feb. 2022 by 400 MHz air-coupled antennas, and the Hilbert transform was chosen to compute the instantaneous frequency of the decoupled modes. The instantaneous frequency of the GPR signal was established based on the optimized VMD. The spectra of GPR signal based on optimized VMD method were applied to evaluate dry and wet fouled ballast in field test and compared the conventional TF spectrum methods and illustrated the superiority. The experimental results of GPR with dry and wet fouled ballasts demonstrate that, by comparison with the feature extraction method of conventional spectrum methods such as spectrogram and wavelet, the feature extraction method based on the optimized VMD has much better separability and quantitative identification capability.

The rest of this paper is structured as follows. Section 2 presents the theoretical background of the optimized VMD algorithm and introduces the specific steps of the optimized VMD algorithm. Section 3 presents the field experiment details, including GPR equipment, test site, materials/real ballast in railway, and main steps of the proposed fault feature extraction method. Section 4 carries out the signal processing and compares the results of the optimized VMD algorithm with spectrogram and wavelet results. Section 5 gives the conclusion of this paper.

2. Theoretical Background

2.1. Basic Theory for the Variational Mode Decomposition (VMD) Method. VMD is a method for the decomposition of the nonrecursive signal. This method can decompose a real-valued input nonlinear signal into a series of modes [15]. Through the VMD method, the signal $f(t)$ can be decomposed into n number of intrinsic mode functions (IMF).

$$f(t) = \sum_{k=1}^{n} u_k(t). \tag{1}$$

Each mode can be defined by the following equations (the amplitude-frequency modulation signal):

$$u_i(t) = A_i(t)\cos\left[\varphi_i(t)\right], \tag{2}$$

where $u_i(t)$ represents the ith mode; $A_i(t)$ represents the instantaneous amplitude; $\varphi_i(t)$ represents the instantaneous phase. Define $\omega_i(t) = \varphi_{i'}(t)$ as the instantaneous frequency. Both $A_i(t)$ and $\omega_i(t)$ vary much slower than $\varphi_i(t)$. Thus, over a sufficiently long interval $[t-\eta, t+\eta]$, where $\eta = 2\pi/\omega_i$ (t), the mode $u_i(t)$ can be considered as a pure harmonic signal. The amplitude of that is $A_i(t)$, and the instantaneous frequency is $\omega_i(t)$. The core function of VMD is to calculate the center frequency and bandwidth of the extracted modes to display different components in the signal. Each mode is closely surrounded the center pulsation ω_i, and its bandwidth can be calculated by the squared $L2$-norm of the gradient. VMD can be expressed by following equations that are solving the solution of a constrained variational problem:

$$\begin{aligned} &\min_{\{u_i\},\{w_i\}} \left\{ \sum_{i=1}^{k} \left\| \partial_t \left[\left(\delta(t) + \frac{j}{\pi t} \right) * u_i(t) \right] e^{-jw_i t} \right\|_2^2 \right\}, \\ &\text{s.t. } x(t) = \sum_{i=1}^{k} u_i(t), \end{aligned} \tag{3}$$

where K represents the number of modes; $\{u_i\} = \{u_1, u_2, \ldots, u_k\}$ represents the set of estimated modes; $\{\omega_i\} = \{\omega_1, \omega_2, \ldots, \omega_k\}$ represents the set of center frequencies that corresponds to the estimated modes; ∂t represents the gradient function; $\delta(t)$ represents the Dirac distribution. Through the Lagrangian multiplier λ and the quadratic penalty factor α, the constrained variational problem degraded into an unconstrained problem which can be described by the augmented Lagrangian function presented as follows:

$$\begin{aligned} L(\{u_i\},\{w_i\},\lambda) = {} & \alpha \sum_{i=1}^{k} \left\| \partial_t \left[\left(\delta(t) + \frac{j}{\pi t} \right) * u_i(t) \right] e^{-jw_i t} \right\|_2^2 \\ & + \left\| f(t) - \sum_{i=1}^{k} u_i(t) \right\|_2^2 \\ & + \left\langle \lambda(t), f(t) - \sum_{i=1}^{k} u_i(t) \right\rangle. \end{aligned} \tag{4}$$

This problem can be solved by searching the saddle point of the above equation. The way to find that point is using the alternate direction method of multipliers. From (3), we can summarize the modes in the frequency domain by updating each mode u_i and its center frequency ω_i constantly:

$$\begin{aligned} \hat{u}_i^{n+1}(\omega) &= \frac{\hat{x}(\omega) - \sum_{j \neq i} \hat{u}_j(\omega) + \lambda(\omega)/2}{1 + 2\alpha(\omega - \omega_i)^2}, \\ \omega_i^{n+1} &= \frac{\int_0^{\infty} \omega |\hat{u}(\omega)|^2 \mathrm{d}\omega}{\int_0^{\infty} \left| \hat{u}_i(\omega) \right|^2 \mathrm{d}\omega}, \end{aligned} \tag{5}$$

where n represents the number of iterations. The operator λ of the Lagrange algorithm is represented as follows:

$$\hat{\lambda}^{n+1}(\omega) = \hat{\lambda}^{n}(\omega) + \tau \left[\hat{x}(\omega) - \sum_{i=1}^{K} \hat{u}_i^{n+1}(\omega) \right]. \tag{6}$$

The above equation will not terminate until the following equation is true:

$$\sum_{i=1}^{K} \frac{\left\| \hat{u}_i^{n+1} - \hat{u}_i^{n} \right\|_2^2}{\left\| \hat{u}_i^{n} \right\|_2^2} < \varepsilon. \tag{7}$$

The four parameters, which are the noise tolerance τ, the convergence error ε, the modal component number K, and the quadratic penalty factor α, must be prepared firstly before using the VMD method. Since the parameter K represents the number of modes and α represents the bandwidth and the center frequency, they have much more

influence on the result of decomposition; therefore, it is crucial to optimize these two parameters. As for the other two parameters τ and ε, they can be set according to fixed default values.

2.2. Instantaneous Amplitude and Frequency. The next step is to apply the Hilbert transform to all IMFs $u_j(t)$ which is expressed as

$$H\left[u_j(t)\right] = \frac{1}{\pi}\int_{-\infty}^{\infty}\frac{u_j(t)}{t-\tau}\mathrm{d}\tau, \quad H\left[u_j(t)\right] = \frac{1}{\pi}\int_{-\infty}^{\infty}\frac{u_j(t)}{t-\tau}\mathrm{d}\tau, \tag{8}$$

where τ represents time. The complex signal can be expressed as

$$Z_j(t) = u_j(t) + iH\left[u_j(t)\right] = a(t)e^{i\phi(t)}. \tag{9}$$

In (9), which expresses a signal, the amplitude and phase can be expressed as

$$a_j(t) = \sqrt{\left[u_j(t)\right]^2 + H\left[u_j(t)\right]}, \quad \phi_j(t) = \arctan\left\{\frac{H\left[u_j(t)\right]}{u_j(t)}\right\}, \tag{10}$$

where $a_j(t)$ is the amplitude, and $\phi_j(t)$ is the phase of the signal. Then, the instantaneous frequency of the signal $\omega(t)$ can be expressed as

$$\omega(t) = \frac{d\phi(t)}{dt}. \tag{11}$$

Then, $f(t)$ can be expressed as

$$f(t) = \sum_{j=1}^{n} a_j(t)\exp\left[i\omega_j(t)\right]. \tag{12}$$

The formula (12) can be extended so that the Hilbert instantaneous frequency $H(t,\omega)$ can be expressed as

$$H(t,\omega) = \mathrm{Re}\left\{\sum_{j=1}^{n} a_j(t)\exp\left[i\int\omega_j(t)\mathrm{d}t\right]\right\}, \tag{13}$$

where t and ω represent time and frequency, respectively.

Due to mean zero and the local symmetry property, the IMFs obtained from the equations above are able to assure the physical meanings of the instantaneous frequencies. Instantaneous attributes of GPR data can be extracted from the IMF and its Hilbert transform.

2.3. Optimization of VMD. Selecting the suitable parameters, especially the number of decomposed components for VMD is a critical task. GPR signals are vulnerable to be contaminated by interferences such as background noise and electromagnetic factors. These interferences can smear the fault-related features contained in the signals. Therefore, it is crucial and essential to minimize undesirable influences. The optimization of the number of modes for reaching such a purpose has been investigated [16, 17]. Considering the fact that the magnitude of the frequency spectrum of these interferences is often smaller compared to that of valid frequency components, a method based on spectrum envelope has been used to identify the valid frequency components contained in the signal, by which the optimum number of modes of the VMD is determined [12, 17]. This method can be expressed by applying the Fourier transform to the GPR signal.

$$H(\omega) = \int_{-\infty}^{\infty} f(t)e^{-iwx}\mathrm{d}t, \quad Aax = |H(\omega)|.\,(i = 1, 2, \ldots l), \tag{14}$$

where l represents the integer equal to half amount of data. Then, search the local maximum and local minimum magnitudes Aax, and finally, generate the envelope curve of the filtered spectrum by using an interpolation method to calculate appropriate thresholds *Th*.

$$Th = Al + r(Ah - Al), \tag{15}$$

where *Ah* and *Al*, respectively, represent the maximum and minimum magnitudes obtained from the spectrum; *r* represents the ratio for the control of the level of the threshold; in other words, the variation trend of the value *r* is the same as that of the threshold.

Finally, frequency components whose magnitude is smaller than the threshold will be picked out, and the optimum number of modes from the resultant envelope curve for optimized VMD analysis will be identified.

3. Field Validation

The above technique is validated for the GPR signal of ballasts using field data collected in a railway depot in Huntington WV in Feb 2022. The experiment contains two different fouling cases, which are dry and wet, respectively, for the ballast. The test site was investigated using a 400 MHz frequency GPR horn antenna system which was towed along the rail sections through a dedicated cart that allowed the antenna works. Specifically, a 100 feet-long railway section was used. The GPR data collected were analyzed to validate the aforementioned method. For comparison, we also conduct JTFA and wavelet transforms of the tested GPA signal, with the corresponding calculated frequency spectra for the case of dry and wet fouled ballast conditions.

3.1. Test Site. The test item is a 100 feet-long section of the railway. The location and schematic characteristics of the test site are shown in Figures 1(a) and 1(b). The superstructures are composed of steel rails with the distance between the rails on a running line being 4′ 8.5″. The railway fastened to wood sleepers with the crosstie spacing of mainline railroad 19″.

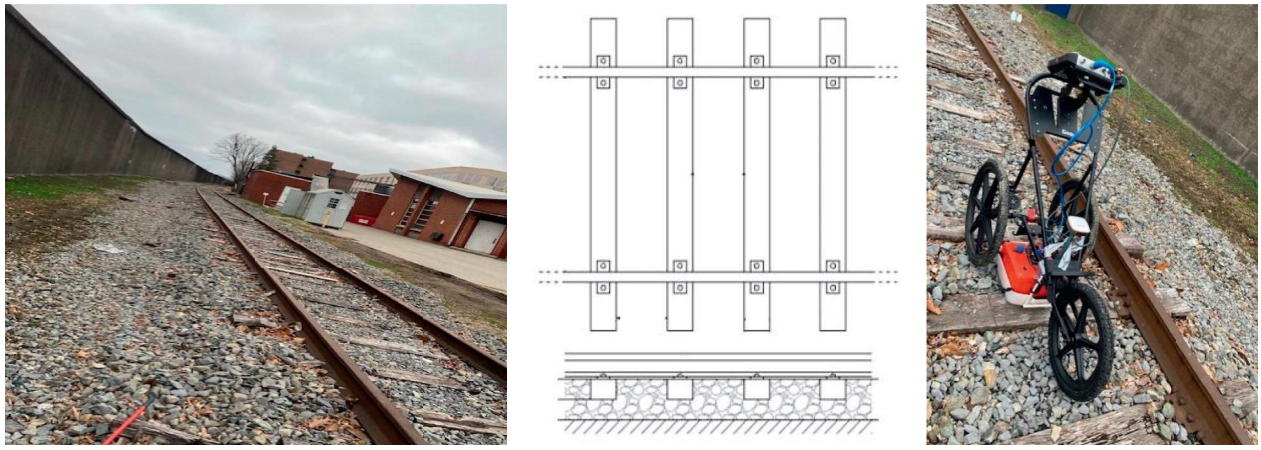

(a) (b) (c)

Figure 1: (a) Location of the test site. (b) Schematic characteristics of the railway. (c) Test equipment GPR.

3.2. Equipment of the Test. Different EM responses from different configurations were investigated by towing a pulsed GPR system equipped with high-frequency horn antennas manufactured by RT Clark Company along the test site. The central frequency of the antennas is 400 MHz. The surveys were conducted through a hand-towed cart shown in Figure 1(c). The GPR antennas were suspended in the air at a height of 1 cm beyond the ballast surface through a plastic support laying on a hand-towed cart for railway track study.

3.3. Materials. Based on the inspection, the existing ballast in the site is attributed to be a kind of highly fouled type. Two types of ballasts were arranged in the test samples, namely, the existing railway dry ballasts and then the wet ballasts that were generated by applying 3-gallon water into existing dry ballasts enclosed by two rails and two sleepers in the test site. Data collection was carried out two times when the ballasts are dry and wet, respectively. All the collections are operated by towing the GPR system along the full test-site area.

4. Results and Discussion

The raw data of GPR signal are processed through Fourier transform, short-time Fourier transform method, and discrete wavelet transform method. Figure 2 illustrates the GPR signal of dry ballast and the FFT spectrum.

Figure 3 shows the spectrogram of the GPR signal of dry ballast and the wavelet spectrum.

In Figure 2(b), FFT spectrum of GPR signal of dry ballast, there exists wideband, multiple peaks of coupled modes (four peaks which could be assumed to be four coupled modes). This indicates the heavily fouling condition.

It is noted that based on existing research, the clean fresh ballast usually exhibits a spectrum with one peak with a relatively much wider band than fouled one [18]. The existing research also demonstrated that the highly fouled ballast or ballast with highly different-sized aggregates usually exhibits a spectrum with multiple peaks [10].

The time-frequency analysis, which is depicted in Figure 3, demonstrates that most of the energy is focused on a short arrival time, approximately 5 ns, followed by a gradual attenuation ending up around 20 ns.

The influence of wet condition on the spectrum of the ballast is shown in the following figures.

Figure 4 shows the GPR signal of wet ballast and the FFT spectrum. Figure 5 shows the spectrogram of the GPR signal of wet ballast and the wavelet spectrum.

For comparison, the following figure puts the GPR signal and FFT spectra of dry and wet ballast together, respectively. Figure 6 shows GPR signals of dry ballast vs wet ballast and the FFT spectra of GPR of dry ballast vs wet ballast.

From the GPR signals recorded over the dry and wet cases in Figure 6(a), it is clear that the wet condition influences the overall responses. On the other hand, it is noticed that wet condition causes big differences in the signals in the frequency domains in Figure 6(b), as reported in previous studies in the literature.

In Figure 6(b), there exist the complex features of wet ballast spectrum compared with dry ballast spectrum: a. peak frequency shift of specific frequency component or specific mode; b. attenuation of the peak of a specific mode; c. the area changes of the spectrum of a specific mode. It is noted that the above changes in the peak shift/attenuation/area are not consistent for different four modes.

Comparison of the peak shifts of the modes in the spectrum, the peaks of the first three modes of the wet ballast shift to a lower frequency end, whereas the peak of the last mode of the wet ballast is identical to its dry case.

Comparison of the peak attenuations of the modes in the spectrum, the peaks of the first two modes of the dry ballast are higher than their wet cases, respectively, whereas the peaks of the last two modes of the dry ballast are lower than their wet cases, respectively.

Comparison of the area changes in the spectrum of the modes, the areas of the first two modes of the wet ballast are smaller than that of the dry ballast, respectively, whereas the areas of the last two modes of the wet ballast are larger than that of the dry cases, respectively.

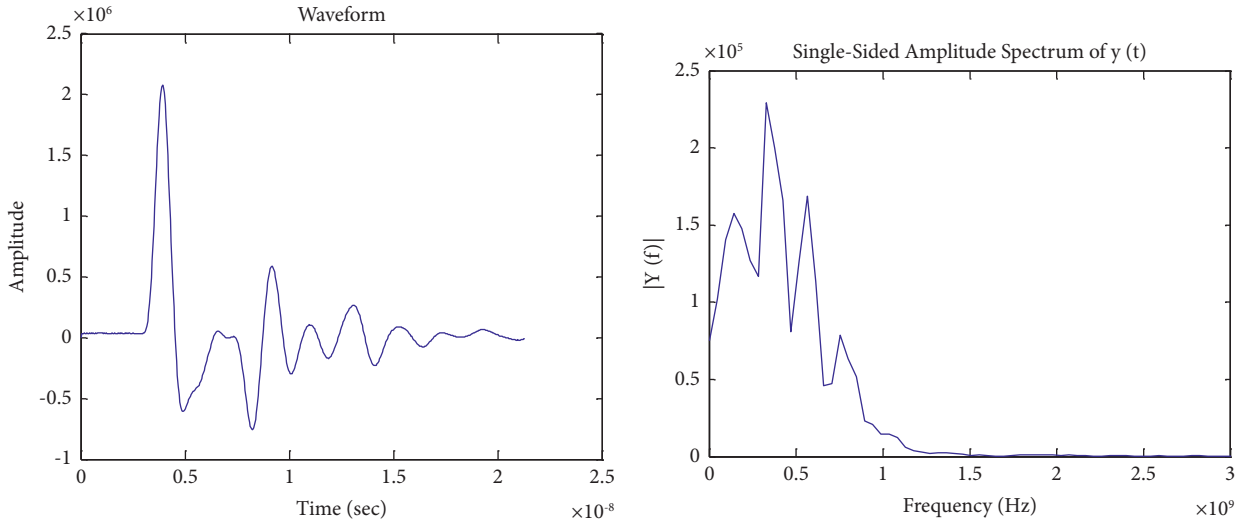

Figure 2: (a) GPR signal of dry ballast. (b) FFT spectrum of GPR signal of dry ballast.

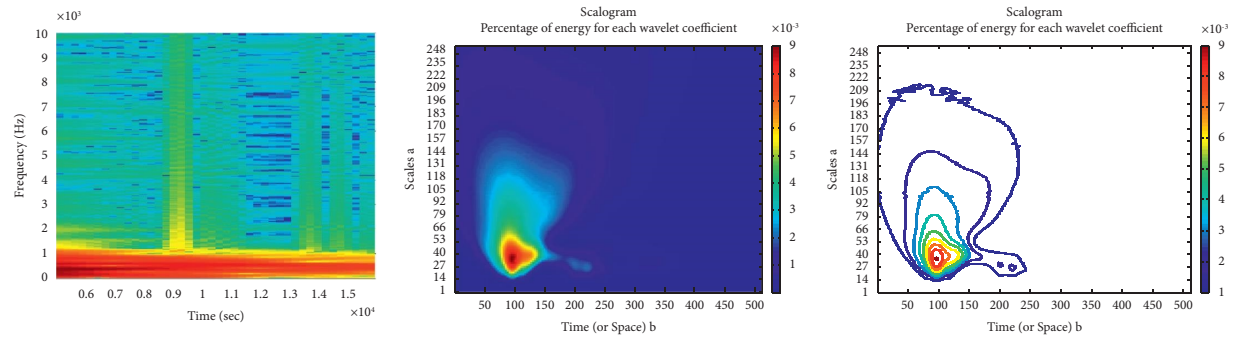

Figure 3: (a) Spectrogram of GPR signal of dry ballast. (b), (c) Wavelet spectrum of GPR signal of dry ballast.

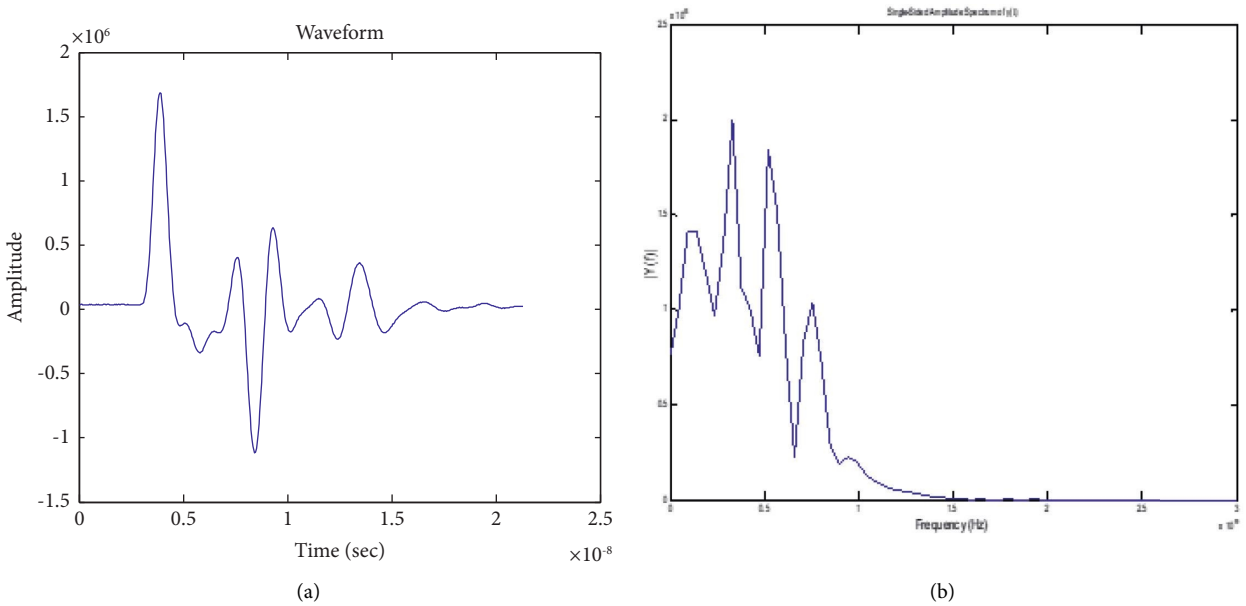

Figure 4: (a) GPR signal of wet ballast. (b) FFT spectrum of GPR signal of wet ballast.

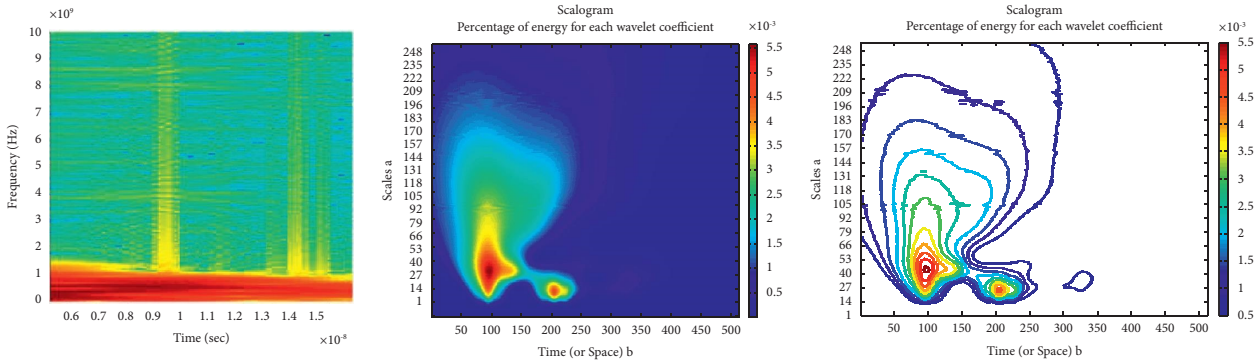

(a) (b) (c)

Figure 5: (a) Spectrogram of GPR signal of wet ballast. (b), (c) Wavelet spectrum of GPR signal of wet ballast.

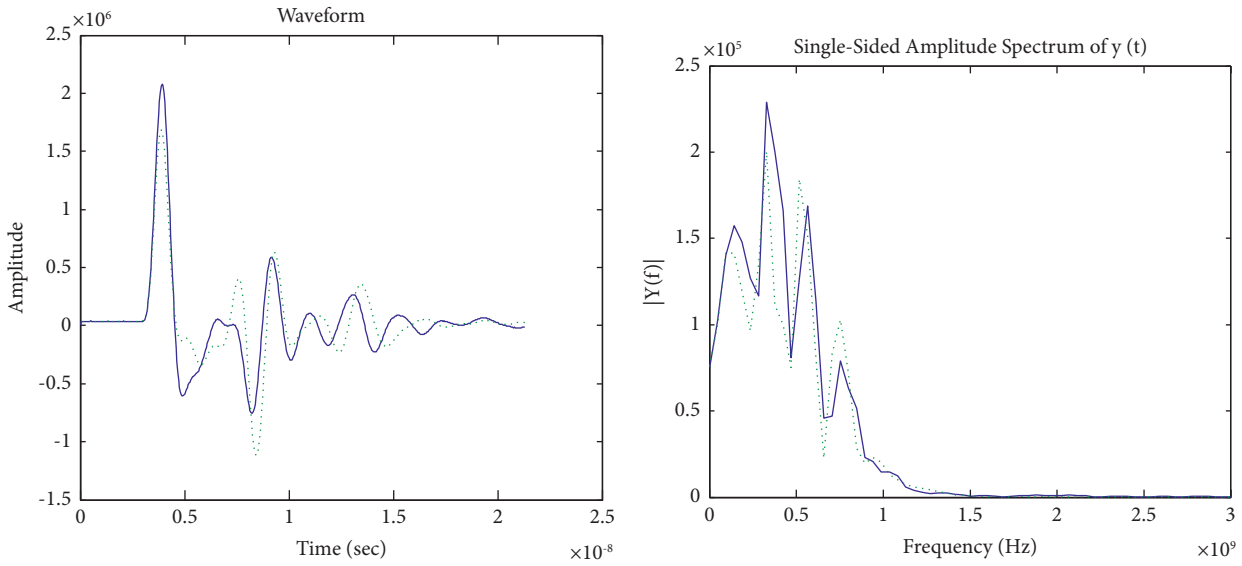

(a) (b)

Figure 6: (a) GPR signals of dry ballast vs wet ballast (solid line: dry; dotted line: wet). (b) FFT of GPR signals of dry ballast vs wet ballast (solid line: dry; dotted line: wet).

It is noted that many existing research used the spectrum area change or peak shift of GPR signal as criteria for ballast analysis. In the existing research, the spectrum of GPR signal exhibits a single wide mode for clean ballasts that were well prepared in the lab, and the spectrum changes toward a lower frequency end and smaller area for fouled ballast. However, the real fouled ballast exhibits diversified trends due to multiple mode interactions. This renders the difficulty to select criteria to setup the evaluation index in the real application.

Many existing research used spectrogram and wavelet spectrum of GPA such as in Figures 3 and 5 to distinguish the attribute changes of ballast under different conditions. It should be noticed that the energy attenuation can only be observed qualitatively in the spectrogram and wavelet spectrum by comparing the color change rate from the hot color that represents high energy to cool color that represents low energy. Al-Qadi et al. [9] proposed to use the spectrogram to analyze the levels of the fouling conditions for ballast by comparing different speeds among the energy attenuations [9]. They also illustrated that it is possible to make use of the wavelet coefficient of wavelet transform to reconstruct the original signal to distinguish fouling levels, but reliable criteria need to be established.

Figure 7 shows the Hilbert spectrum of the decoupled modes GPR with optimized VMD of dry ballast and wet ballast.

Based on Figure 7, the comparison of the Hilbert spectrum of optimized VMD GPR from dry and wet ballast, we can see that there exists a very clear difference between specific mode frequency of dry and wet ballast. As such, it is very clear and easy to use specific mode frequency to form an assessment index and use its shift as reliable and robust criteria to assess the changes in the properties of ballast, which obviously overperform that of

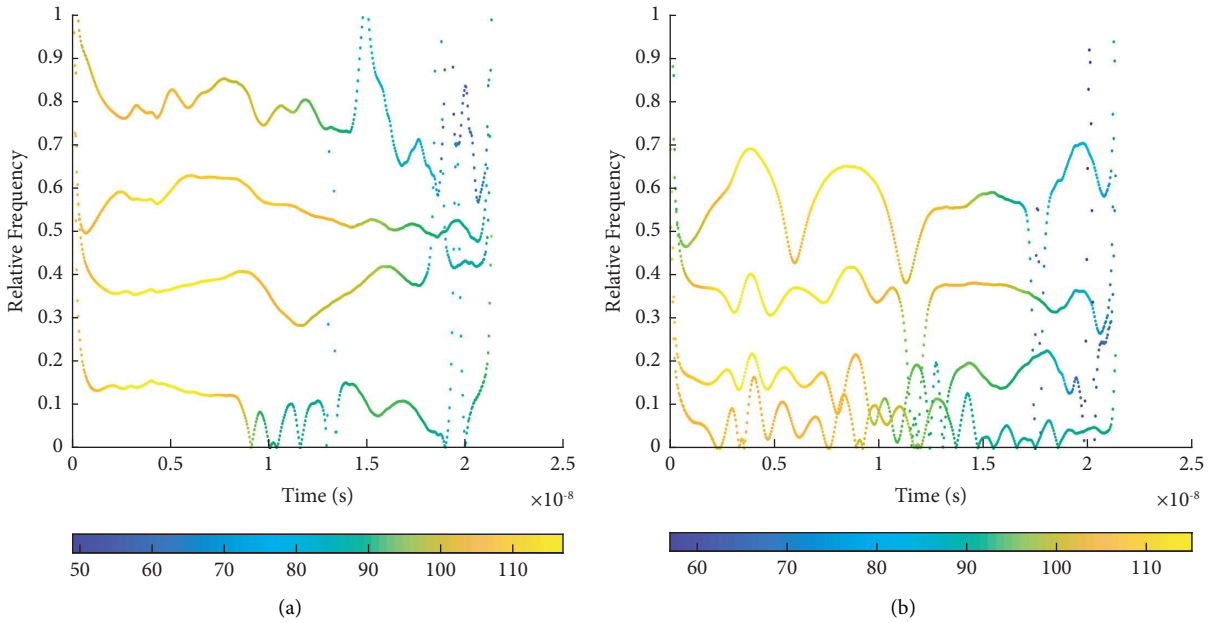

Figure 7: Hilbert spectrum of the modes from optimized VMD GPR of dry ballast (a). Wet ballast (b).

the conventional methods as illustrated in Figures 2–6. This method can also be extended for quantifying the water contents in other materials such as sand, soil, and concrete which had been assessed by using conventional spectra of GPR signals [22–26]. Moreover, this method can be further improved by incorporating the advanced optimization and artificial intelligence methods [19–21, 26, 27]. It is noted that several advanced approaches such as EMD, EEMD, CEEMDAN, LMD, and ITD have been developed and used to process complicated signals, some of which could be competitive to VMD in specific applications. However, compared with EMD, EEMD, CEEMDAN, LMD, and ITD, VMD has a strong mathematical theory basis [28–30].

5. Conclusion

This paper uses the optimized variational mode decomposition method to decouple the complex nonlinear modes of the GPR signal of ballast for condition assessment. The proposed advanced time-frequency analysis overperforms the conventional spectrum and time-frequency analysis of GPR signal by giving quantitative evaluation to the assessment of ballast conditions.

The results of the water content effect on ballast GPR signal spectrum changes in both peaks and areas are consistent with all published research. The decoupled nonlinear modes of GPR signal from optimized VMD are much easier to be used to establish a new condition assessment index for quantifying railway ballast fouling conditions, which is better than all the previously used spectrum methods. The works can be further improved by incorporating advanced optimization algorithms and artificial intelligence algorithms into the VMD for accurate assessment of fouling ballast in the future.

Data Availability

The data used to support the findings of this study will be made available on request.

Conflicts of Interest

The authors declare that they have no conflicts of interest.

Acknowledgments

This research was made possible by US Engineer Research and Development Center (ERDC), Grant nos. W912HZ-19-C-0023 and W81EWF-20-SOI-0036.

References

[1] T. Saarenketo and T. Scullion, "Using Electrical Properties to Classify the Strength Properties of Base Course Aggregates," Texas Transportation Institute, College Station, TX, FHWAITX-9711341-2, 1995.

[2] R. M. Narayanan, J. W. Jakub, D. Li, S. E. Elias, and G. Eliasa, "Railroad track modulus estimation using ground penetrating radar measurements," *NDT&E International*, vol. 37, no. 2, pp. 141–151, 2004.

[3] H. Huang, E. Tutumluer, and W. Dombrow, "Laboratory Characterization of Fouled Railroad Ballast Behavior," *Transportation Research Record: Journal of the Transportation Research Board*, vol. 2117, pp. 93–101, 2009.

[4] D. B. Robert, "Non-Destructive Evaluation of Railway Trackbed Ballast," The University of Edinburgh, Edinburgh UK, Doctor of Philosophy, 2011.

[5] F. K. Hamed, "Evaluating the Influence of Br Aluating the Influence of Breakdown Fouling and Moistur Ouling and Moisture Content on Mechanical and Electromagnetic Properties of Ballasted Railroad Track," Ph.D. Thesis,

University of Massachusetts Amherst, Amherst, MA 01003, USA, 2017.

[6] M. Silvast, M. Levomaki, A. Nurmikolu, and J. Noukka, "NDT techniques in railway structure analysis," in *Proceedings of the 7th World Congress on Railway Research*, Montreal, Quebec,Canada, June 2006.

[7] Z. Leng and I. L. Al-Qadi, "Railroad ballast evaluation using ground-penetrating radar," *Transportation Research Record: Journal of the Transportation Research Board*, vol. 8, no. 1, pp. 110–117, 2010.

[8] W. Shao, A. Bouzerdoum, S. L. Phung, L. Su, B. Indraratna, and C. Rujikiatkamjorn, "Automatic classification of ground-penetrating-radar signals for railway-ballast assessment," *IEEE Transactions on Geoscience and Remote Sensing*, vol. 11, no. 10, pp. 3961–3972, 2011.

[9] I. L. Al-Qadi, S. Zhao, and P. Shangguan, "Railway Ballast Fouling Detection Using GPR Data: Introducing a Combined Time–Frequency and Discrete Wavelet Techniques," *Near Surface Geophysics*, vol. 14, pp. 145–153, 2016.

[10] L. Bianchini Ciampoli, F. Tosti, M. G. Brancadoro, F. D'Amico, A. M. Alani, and A. Benedetto, "A spectral analysis of ground-penetrating radar data for the assessment of the railway ballast geometric properties," *NDT & E International*, vol. 90, pp. 39–47, 2017.

[11] S. Fontul, A. Paixão, M. Solla, and L. Pajewski, "Railway track condition assessment at network level by frequency domain analysis of GPR data," *Remote Sensing*, vol. 10, no. 4, p. 559, 2018.

[12] F. N. Birhane, Y. T. Choi, and S. J. Lee, "Development of condition assessment index of ballast track using ground-penetrating radar (GPR)," *Sensors*, vol. 21, no. 20, p. 6875, 2021.

[13] W. He, T. Hao, H. Ke, W. Zheng, and K. Lin, "Joint time-frequency analysis of ground penetrating radar data based on variational mode decomposition," *Journal of Applied Geophysics*, vol. 181, no. 19, pp. 104146–104148, 2020.

[14] J. Xu and B. Lei, "Data interpretation technology of GPR survey based on variational mode decomposition," *Applied Sciences*, vol. 9, no. 10, p. 2017, 2019.

[15] K. Dragomiretskiy and D. Zosso, "Variational mode decomposition," *IEEE Transactions on Signal Processing*, vol. 62, no. 3, pp. 531–544, 2014.

[16] S. Liu, G. Tang, X. Wang, and Y. He, "Time-frequency analysis based on improved variational mode decomposition and Teager energy operator for rotor system fault diagnosis," *Mathematical Problems in Engineering*, vol. 2016, pp. 1–9, 2016.

[17] P. Shi and W. Yang, "Precise feature extraction from wind turbine condition monitoring signals by using optimised variational mode decomposition," *IET Renewable Power Generation*, vol. 11, no. 3, pp. 245–252, 2017.

[18] M. F. Isham, M. S. Leong, M. H. Lim, and M. K. Zakaria, "A review on variational mode decomposition for rotating machinery diagnosis," *MATEC Web of Conferences*, vol. 255, p. 02017, 2019.

[19] Y. Li, B. Tang, X. Jiang, and Y. Yi, "Bearing fault feature extraction method based on GA-VMD and center frequency," *Mathematical Problems in Engineering*, vol. 2022, pp. 1–19, Article ID 2058258, 2022.

[20] Y. Li, L. Mu, and P. Gao, "Particle swarm optimization fractional slope entropy: a new time series complexity indicator for bearing fault diagnosis," *Fractal Fract*, vol. 6, no. 7, p. 345, 2022.

[21] Q. Ni, J. C. Ji, K. Feng, and B. Halkon, "A fault information-guided variational mode decomposition (FIVMD) method for rolling element bearings diagnosis," *Mechanical Systems and Signal Processing*, vol. 164, no. 1, Article ID 108216, 2022.

[22] R. A. Federal, "Ground Penetrating Radar Technology Evaluation on the High Tonnage Loop: Phase 1," Federal Railroad Administration, Washington, DC 20590 USA, DOT/FRA/ORD-17/18, 2017.

[23] Y. S. Yan, Y. Yan, and G. Zhao, "Estimation of sand water content using GPR combined time-frequency analysis in the Ordos Basin," *Open Physics*, vol. 17, pp. 999–1007, 2019.

[24] F. Tosti and E. Slob, "Determination, by using GPR, of the volumetric water content in structures, sub-structures, foundations and soil – ongoing activities in Working Project of COST action TU1208," in *Civil Engineering Applications of Ground Penetrating Radar*, A. Benedetto and L. Pajewski, Eds., Springer, Heidelberg, Germany, 2015.

[25] W. Zatar, T. T. Nguyen, and H. Nguyen, "Environmental effects on condition assessments of concrete structures with ground penetrating radar," *Journal of Applied Geophysics*, vol. 203, Article ID 104713, 2022.

[26] W. Zatar, T. T. Nguyen, and H. Nguyen, "Predicting GPR signals from concrete structures using artificial intelligence-based method," *Advances in Civil Engineering*, vol. 2021, pp. 1–9, Article ID 6610805, 2021.

[27] W. A. Zatar, M. A. Alzarrad, T. T. Nguyen, and H. D. Nguyen, *Artificial Neural Network Utilization for Nondestructive Testing and Evaluation of Concrete Structures*, vol. 350, pp. 167–177, Special Publication, USA, 2021.

[28] J. Mei, G. Ren, J. Jia, X. Jia, J. Han, and Y. Wang, "An improved variational mode decomposition method and its application in diesel engine fault diagnosis," *JOURNAL OF VIBROENGINEERING*, vol. 20, no. 6, pp. 2363–2378, 2018.

[29] Z. Wang, J. Wang, Y. Kou, J. Zhang, S. Ning, and Z. Zhao, "Weak fault diagnosis of wind turbine gearboxes based on MED-LMD," *Entropy*, vol. 19, no. 6, p. 277, 2017.

[30] S. Hadiyoso, E. M. Dewi, and I. Wijayanto, "Comparison of EMD, VMD and EEMD methods in respiration wave extraction based on PPG waves," *Journal of Physics: Conf. Ser.*vol. 1577, no. 1, Article ID 012040, 2020.